Nuclear Inst, and Methods in Physics Research B 428 (2018) 17–23

Contents lists available at ScienceDirect

Nuclear Inst. and Methods in Physics Research B

journal homepage: www.elsevier.com/locate/nimb

Microstructural evolution and mechanical properties in $Cu_{48}Zr_{48}Al_4$ bulk metallic glass composites induced by He^+ ion irradiation

Yuhang Wei[a,b], Kun Zhang[a,b], Bingchen Wei[a,b,*], Ziqiang Zhao[c], Junming Yuan[d]

[a] Key Laboratory of Microgravity (National Microgravity Laboratory), Institute of Mechanics, Chinese Academy of Sciences, Beijing 100190, China
[b] School of Engineering Science, University of Chinese Academy of Sciences, Beijing 101408, China
[c] School of Physics, Peking University, Beijing 100871, China
[d] School of Environment and Safety Engineering, North university of China, Taiyuan 030051, China

ARTICLE INFO

Keywords:
Ion irradiation
Metallic glass composites
Martensitic transformation
Nanoindentation

ABSTRACT

The irradiation-induced phase transformation and mechanical property stability of the $Cu_{48}Zr_{48}Al_4$ bulk metallic glass composites (BMGCs) were investigated. An obvious structural transformation occurred from the B2-CuZr phase to the B19′-CuZr and the B33-CuZr phases following irradiation, when the dose increased from 2.5×10^{17} ions/cm^2 to 1.0×10^{18} ions/cm^2. This change was accompanied by the changes of the maximum displacement per atomic (DPA) increasing from 21.5 dpa to 86 dpa. The mean surface roughness increased as the incident dose increased. The local exfoliation occurred at the maximal dose. The changes of mechanical properties were characterized via nanoindentation. The hardness and Young's modulus in the amorphous regions decreased as the dose increased. In contrast, the crystalline regions presented a distinct hardening effect, due to the appearance of the martensitic phases. The macroscopic hardness of the BMGCs obtained by the Vickers indentation instrument was basically unchanged after irradiation. The results suggested that these materials maintained a stable performance, because of the combined effects of hardening and softening. This study could aid the design of novel materials that are subjected to irradiation circumstance.

1. Introduction

The development of the first-wall materials within fusion reactors is an ongoing process [1,2]. The long-term irradiation circumstance results in the structure alloys becoming bombarded by thermal neutrons, hydrogen isotope particles, and helium ions. This changes the material's structure and properties, due to the generation of Frenkel pair defects [3]. The gradual accumulation of the microscopic defects forms numerous defect clusters such as dislocation loops, voids and stacking fault tetrahedrons, which ultimately induces an obvious hardening effect [4]. The hardening reduces the ductility of the materials, causes embrittlement [5], as well as shortens the service life when applied in an irradiation environment. Designing novel materials with stable mechanical properties is crucial for these reactors.

Bulk metallic glasses (BMGs) are believed as an ideal potential candidate for applications in nuclear-irradiated environments, as they lack crystalline defects, such as dislocations and grain boundaries [6,7]. Some studies have found that the ion beam resistance capability of the BMGs is greater than the traditional radiation resistance materials [8]. The free volume increases inside the matrix when a high irradiation dose is applied, which could improve the plastic-deformation ability and display a softening effect [9]. However, the BMGs usually failed due to catastrophic fracture, where they exhibit little macro plasticity at room temperature [10]. This would restrict their further application as the structural materials in nuclear industry. Bulk metallic glass composites (BMGCs) consist of a glassy matrix and crystalline phases, where they have been shown to effectively enhance the plasticity of the BMGs [11]. The BMGCs may maintain stable mechanical properties under irradiation, by combining the softening and the hardening effects that occur in the amorphous and crystalline alloys. The work hardening and considerable tensile ductility were obtained in CuZr-based BMGCs via the precipitation of the B2-CuZr phase [12], demonstrating their potential applications in an irradiation environment. The ion bombardment responses of these materials with both amorphous and crystalline phases are worthy of study.

In this work, the effects of 100 keV He^+ ion irradiation on the structure and mechanical properties of a CuZr-based BMGCs were studied, which presented different responses in the amorphous matrix and the embedded crystalline phases at different doses. The results could promote the understanding of the interaction mechanism between the metallic glass composites and the ion beam.

* Corresponding author at: Key Laboratory of Microgravity (National Microgravity Laboratory), Institute of Mechanics, Chinese Academy of Sciences, Beijing 100190, China.
E-mail address: weibc@imech.ac.cn (B. Wei).

https://doi.org/10.1016/j.nimb.2018.05.003
Received 5 February 2018; Received in revised form 30 April 2018; Accepted 1 May 2018
0168-583X/

2. Experimental methods

A $Cu_{48}Zr_{48}Al_4$ alloy with a single B2-CuZr phase embedded in a glass matrix was fabricated by arc melting in an argon atmosphere. The raw materials used for alloy had a purity of 99.99%. The two sides of ingots were completely remelted five times to ensure its chemical composition homogeneity. Cylindrical rods with 5 mm in diameter and 60 mm in length were prepared via suction casting using a copper mold. The samples 2.0 mm in length were cut from the resulting rods. Prior to irradiation experiments, surfaces of the samples were mechanically polished to a mirror finish and cleaned ultrasonically. Next, the polished samples were irradiated with 100 keV He^+ ion beam at normal angle using the BNU-400 kV electrostatic accelerator with a dose of 2.5×10^{17} ions/cm^2, 5.0×10^{17} ions/cm^2 and 1.0×10^{18} ions/cm^2, respectively. SRIM2008 program was used for calculating the ions range and displacement per atom (DPA) in the target materials [13]. After the irradiation experiment, the phase structures of the as-cast and irradiated samples were studied by X-ray diffraction (XRD) using Cu Kα radiation. The microstructure was investigated by optical microscope (OM; Olympus BX-51) and scanning electron microscope (SEM, JEM-2100F). The surface morphology and roughness were characterized by atomic force microscope (AFM, Hysitron Tribo Scope). Nanoindentation experiments were conducted at room temperature (29.0 °C) on Agilent Nano Indenter G200 with a stand Berkovich indenter. Hardness (H) and Young's modulus (E) were measured through the continuous stiffness measurement (CSM) mode (Δh = 2 nm, f = 45 Hz) [14]. Each nanoindentation test ran at a constant strain rate of 0.05 s^{-1} to a maximum of 1000 nm into the indented surface. Vickers hardness tests were done on each sample with a MH-6 digital micro-hardness tester with a load of 100 g (0.98 N) for 10 s.

3. Results and discussion

The simulation of the incident helium ions in $Cu_{48}Zr_{48}Al_4$ BMGC was calculated via SRIM2008. Fig. 1 shows the incident depth-dependent distribution curve for the displacement per atom (DPA), as well as the nuclear and electronic stopping powers induced by 100 keV He ion irradiation (dose = 1.0×10^{18} ions/cm^2). The DPA is an important characterization mean of the irradiation-induced damage on materials [15]. The SRIM simulation details are shown in Table 1 [16]. The damage profile of the $Cu_{48}Zr_{48}Al_4$ was determined from the sum of the predicted Cu, Zr, and Al vacancy concentrations and the replacement events, which was primarily concentrated within 0 μm–0.6 μm from the surface. The DPA in the CuZr-based BMGC increased rapidly, where it reached the maximum of 86 dpa at the depth of 0.35 μm. The peak values of the DPA that corresponded to the doses of 2.5×10^{17} ions/cm^2 and 5.0×10^{17} ions/cm^2 were 21.5 dpa and 43 dpa. The electronic stopping power decreased with the depth increased. While the nuclear stopping power reached the maximum value at the depth of 0.35 μm, and then decreased significantly [17].

Table 1
Input to SRIM 2008 software.

Ion date Symbol	Atomic number	Energy (keV)	Angle of incidence	Target data Displacement energy (eV)	Lattice binding energy (eV)	Surface binding energy (eV)
Cu	29	100	0	30	3	3.52
Zr	40			40	3	6.33
Al	13			27	3	3.36

The phase composition and microstructure that were characterized by XRD examinations and microscopic tests. Fig. 2 shows the XRD patterns of the as-cast and irradiated $Cu_{48}Zr_{48}Al_4$ BMGC at various doses. The XRD results of the as-cast samples revealed sharp crystalline peaks that corresponded to the B2-CuZr phase superimposed on the broad diffraction of the amorphous phases. The three Bragg-peaks of the B2-CuZr phases were located approximately at $2\theta = 38°$, 57°, and 75°. Fig. 3 shows the OM images of the $Cu_{48}Zr_{48}Al_4$ BMGC before and after irradiation. The spherical precipitates of the B2-CuZr phases embedded in the glassy matrix are observed in Fig. 3(a). The volume fraction of the B2-CuZr particles was 28 ± 3 vol%, via the OM images. The peaks of the monoclinic CuZr, $Cu_{10}Zr_7$ and $CuZr_2$ phases appeared at 2.5×10^{17} ions/cm^2. While the diffraction intensity of the B2-CuZr phase significantly decreased. The relative diffraction intensities of the monoclinic phase increased moderately with the disappearance of B2-CuZr phase at 5.0×10^{17} ions/cm^2. The diffraction intensities corresponding to the monoclinic phase were further enhanced at 1.0×10^{18} ions/cm^2. The XRD results suggested that the as-precipitated B2-CuZr phase transformed into the monoclinic phases after ion irradiation, which is accompanied by the formation of $Cu_{10}Zr_7$ and $CuZr_2$ phases. Meanwhile, there were some martensitic lathes inside the irradiated crystalline particles (Fig. 3(b-d)), which suggested the irradiation-induced martensitic transformation. Previous studies show that the precipitated phase in $Cu_{50}Zr_{45}Ti_5$ glassy alloy during irradiation is a mixture of an orthorhombic $Cu_{10}Zr_7$ phase, a tetragonal $CuZr_2$ phase

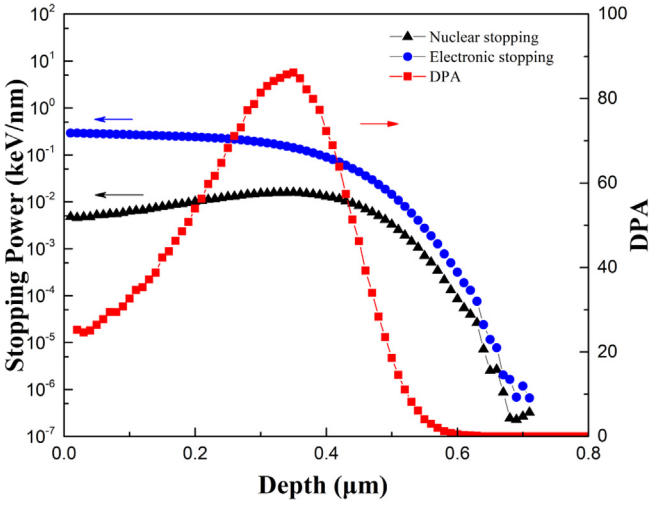

Fig. 1. Distributions of nuclear stopping, electronic stopping and DPA as a function of incident depth at the dose of 1.0×10^{18} ions/cm^2.

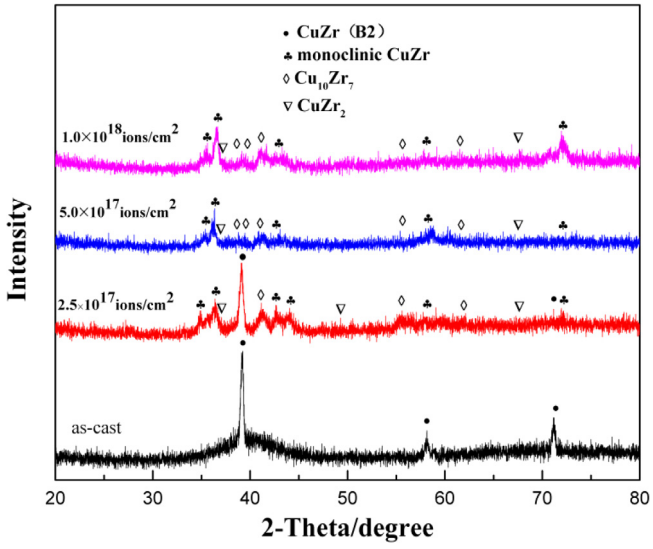

Fig. 2. XRD patterns of the $Cu_{48}Zr_{48}Al_4$ BMGC before and after ion irradiation.

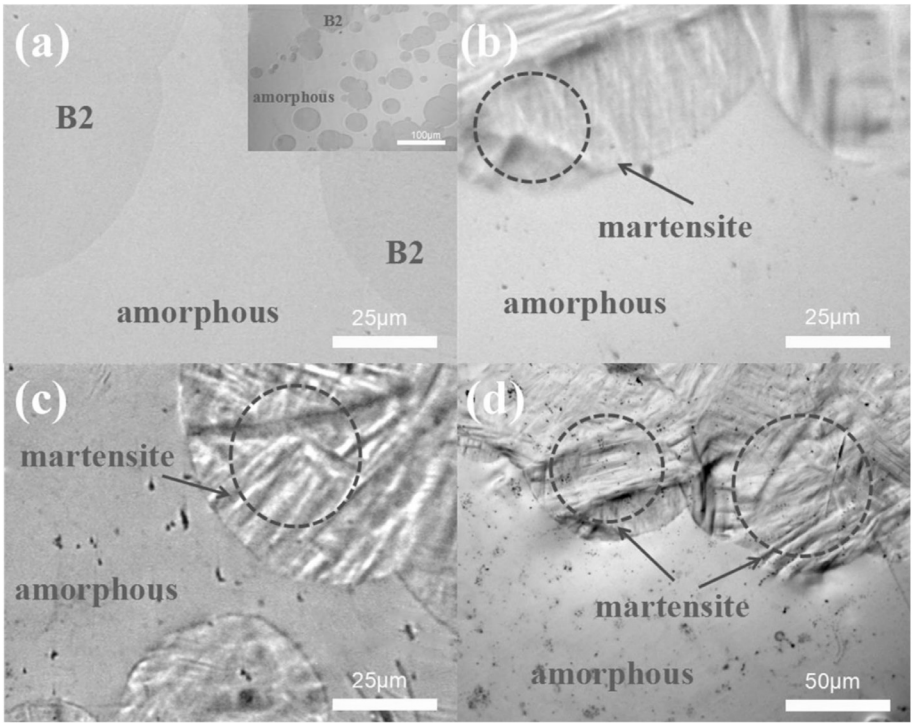

Fig. 3. OM images of the surface of the $Cu_{48}Zr_{48}Al_4$ BMGC samples before and after irradiation at different doses: (a) as-cast, (b) 2.5×10^{17}, (c) 5.0×10^{17} and (d) 1.0×10^{18} ions/cm^2. The inset depicts the surface microstructure of the as-cast sample. The amorphous matrix and the B2 phase (dark contrast) are indicated in the figure. The region marked by the black dashed circle shows the martensitic laths.

and a monoclinic CuZr phase [18]. The formation of the $Cu_{10}Zr_7$ and $CuZr_2$ phases is suggested to via a eutectoid reaction: SCL → $Cu_{10}Zr_7$ + $CuZr_2$ (SCL-supercooled liquid) [3]. However, the formation of the monoclinic CuZr phase is proposed to be due to ion knock-on effect under irradiation. In our paper, the monoclinic CuZr phase is dominated after irradiation due to the ion knock-on effect and irradiation-induced stress [19,20]. We believe that the He^+ ion irradiation may also cause crystallization in the amorphous matrix. As shown in Fig. 2, the precipitated phases are the mixture of the monoclinic CuZr (B19′ and B33), orthorhombic $Cu_{10}Zr_7$ and tetragonal $CuZr_2$ phases. The orthorhombic $Cu_{10}Zr_7$ and tetragonal $CuZr_2$ phases may precipitate from the amorphous matrix.

The AFM images of the surface morphology and the RMS roughness of the amorphous and crystalline regions are depicted in Fig. 4. The sample surface was rougher after irradiation, and the RMS roughness increased when the dose increased. The RMS roughness of the amorphous region reached 7.09 nm at a dose of 2.5×10^{17} ions/cm^2, where some holes appeared on the surface. When the dose increased to 5.0×10^{17} ions/cm^2, the RMS roughness reached 11.2 nm, due to the formation of irradiation-induced damages. At the dose of 1.0×10^{18} ions/cm^2, the RMS roughness reached 22.4 nm due to exfoliation as seen in Fig. 4(a_3). The surface relief phenomenon caused by the appearance of martensitic lath was clearly observed in the crystalline region [21]. Additional B2 phases transformed into monoclinic CuZr phases as the dose increased, which accentuated the effect of the surface relief. The RMS roughness of the crystalline regions increased from 18.1 nm to 48.0 nm, which was greater than the amorphous region at the same dose. The ion irradiation played a dominant role in the roughening process in both amorphous and crystalline regions.

The irradiation-induced damages in the $Cu_{48}Zr_{48}Al_4$ BMGC were further studied by SEM. Fig. 5 shows the surface morphology of the $Cu_{48}Zr_{48}Al_4$ BMGC before and after irradiation. Fig. 5(a) and (e) show that the surface of the amorphous and crystalline regions were flat and smooth before irradiation. A dose of 2.5×10^{17} ions/cm^2 was applied and a few tiny holes appeared in the amorphous region. The crystalline region obtained the martensitic lath and the irradiation-induced damages. When the dose reached 5.0×10^{17} ions/cm^2, the holes in the amorphous region became larger. Some of the martensitic laths were covered by the severe damages in the crystalline region. The irradiation dose was further increased to 1.0×10^{18} ions/cm^2, where the cracking, the exfoliation, and other damages (indicated by the white arrows) appeared in the amorphous regions. A larger exfoliated area (white contrast) appeared in the crystalline regions than in the amorphous regions, which was accompanied by holes, sub-layer exfoliation, and martensitic lath. The exfoliated area expanded further along the boundary when the irradiation dose increased consistently. Usually, the constant bombardment by He^+ ions generated stress among the lattices. The irradiation-induced martensitic transformation was accompanied by the generation of high density dislocations [22,23], which improved the brittleness in the crystalline regions [24]. The results show that the irradiation damage caused by He^+ irradiation in the crystalline region is more severe than that in the amorphous region.

Nanoindentation is usually used to investigate the mechanical behavior of MG systems [25]. The load-displacement (P-h) curves for the amorphous and crystalline regions of the $Cu_{48}Zr_{48}Al_4$ BMGCs are shown in Fig. 6. Fig. 7 shows the hardness and Young's modulus variable trends of the amorphous and crystalline region. The hardness and Young's modulus of the amorphous region decreased from 8.30 GPa to 6.60 GPa and from 124 GPa to 108 GPa, or by 20.4% and 14.3% as shown in Fig. 7(a). This is because the He^+ ion irradiation led to an increased fraction of free volume and caused the extra atomic scale defects [9]. The crystalline regions showed that the peak-load increased as the dose increased from 2.5×10^{17} ions/cm^2 to 1.0×10^{18} ions/cm^2 in Fig. 7(b). The hardness and Young's modulus increased from 6.65

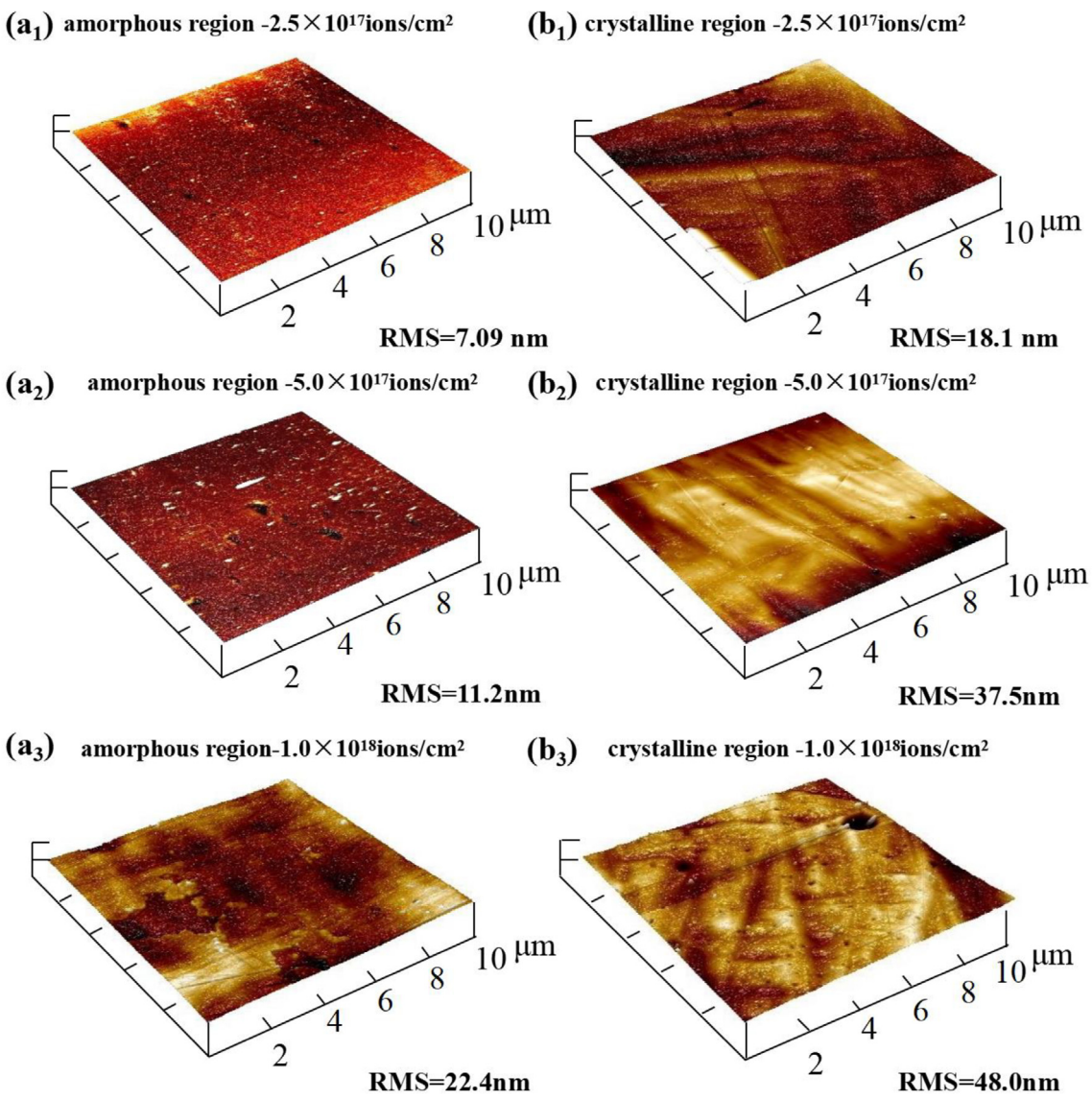

Fig. 4. AFM images of (a_1), (a_2), (a_3) the amorphous regions and (b_1), (b_2), (b_3) the crystalline regions of $Cu_{48}Zr_{48}Al_4$ BMGC with different doses. Here z-scales 30 nm/division.

GPa to 8.04 GPa and from 103 GPa to 115 GPa, due to the formation of the monoclinic martensitic phases [12].

Fig. 8 displays the scattering of the 60 hardness values of the as-cast and the irradiated samples that were irradiated at four irradiation doses. The as-cast sample exhibited a narrow hardness range from 471.22 HV to 481.51 HV, with an average value of 476.55 HV. When the dose reached 2.5×10^{17} ions/cm^2, the hardness was confined within a narrow range, from 464.58 HV to 477.69 HV, with an average value of 470.98 HV. When the dose reached 5.0×10^{17} ions/cm^2, the scatter range of hardness was enlarged, from 469.12 HV to 480.02 HV, with an average value of 474.29 HV. When the dose reached 1.0×10^{18} ions/cm^2, the hardness variation ranged from 461.14 HV to 475.02 HV, with an average value of 469.72 HV. The average hardness value of the sample irradiated at the dose of 1.0×10^{18}ions/cm^2 had the largest variation, at 1.4%. The results showed that the macroscopic hardness values of the $Cu_{48}Zr_{48}Al_4$ BMGC were basically unchanged before and after irradiation.

The surface mechanical properties of the $Cu_{48}Zr_{48}Al_4$ BMGC after ion irradiation were modified, so that the hardness of the amorphous and crystalline regions indicated the opposite tendency. The surface hardness of the irradiated material was caused by a competition between the softening and the hardening, and presented similar Vickers hardness values at the four irradiation doses. This was induced by the increased the free-volume fraction, irradiation-induced damages and the enhanced phases. The $Cu_{48}Zr_{48}Al_4$ BMGC could exhibit stable mechanical properties under the He^+ ion irradiation, due to the combination effects of both the amorphous and crystalline regions. As the irradiation dose increases, the free-volume fraction inside the amorphous matrix increases. However, the precipitation of the nanoparticles in the amorphous region can act as an enhanced phase to prohibit the

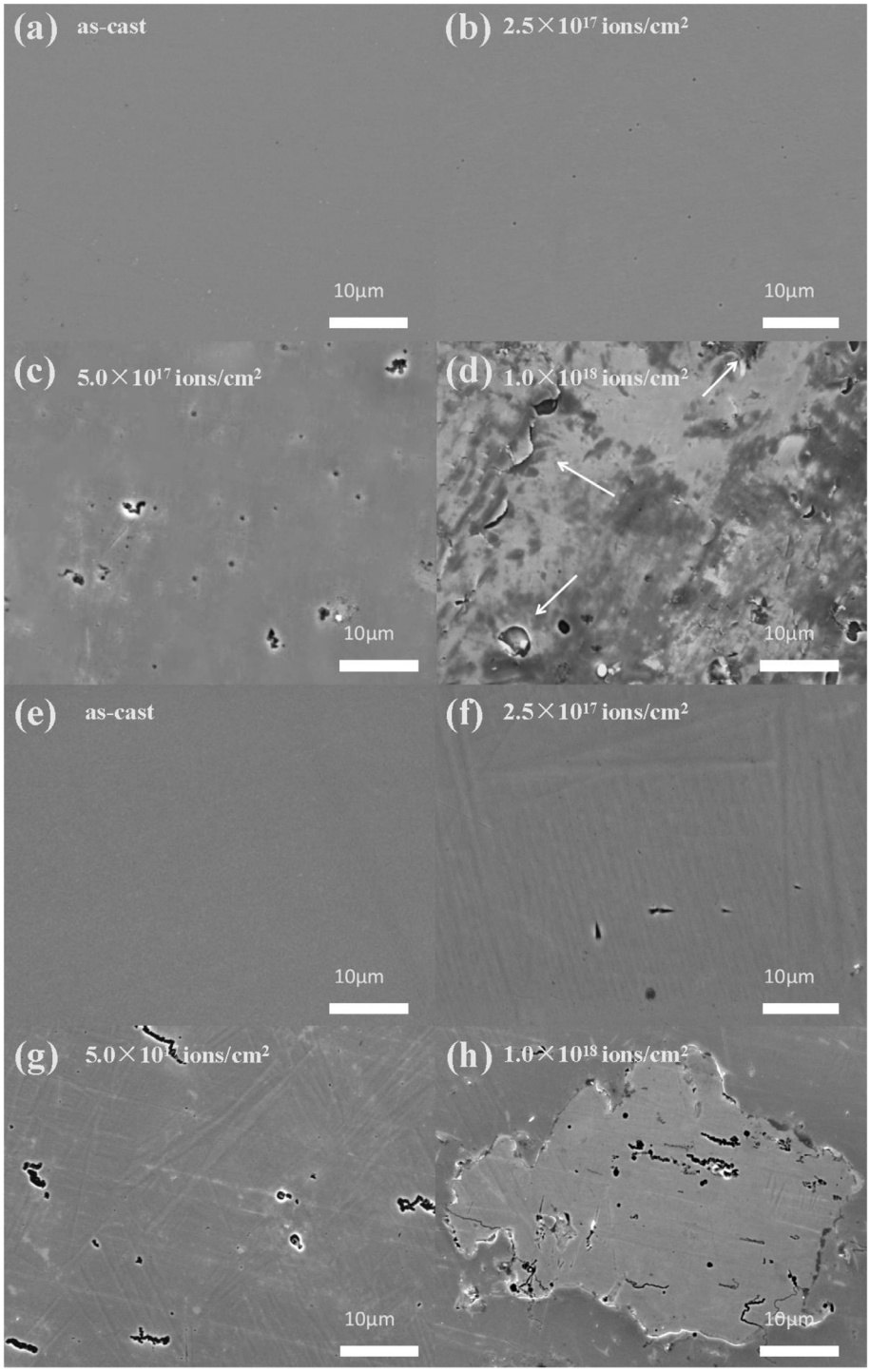

Fig. 5. SEM images of (a), (b), (c), (d) the amorphous region and (e), (f), (g), (h) the crystalline region of $Cu_{48}Zr_{48}Al_4$ BMGC before and after ion irradiation at different doses.

formation and propagation of the shear bands [26]. The softening effect caused by the increase of the free volume and the formation of irradiation-induced defects is greater than the hardening effect caused by the nanoparticles, so the amorphous region behaves an obvious softening phenomenon. However, the B2-CuZr phase undergoes a martensitic transformation from a cubic primitive phase (Pm-3 m) to two monoclinic (P21/m and Cm) phases during the deformation [27,28]. These results revealed a larger hardness value in comparison to the inside regions that maintained the B2-CuZr phase [12]. In my opinion, He^+ ion irradiation could be viewed as a stress-induced process that caused the stress concentration in the main regions of the DPA, therefore, most B2 phases transformed into B19′ and B33 phases after irradiation.

Previous studies [9,29,30] show that ion irradiation could enhance the ductility of BMGs by the increased fraction of free volume. While, the presence of helium bubbles likely reduces the free volume available for plastic deformation. Besides, in Wang's study [9], the ductility of MG pillars has been improved after irradiation, as the irradiation dose

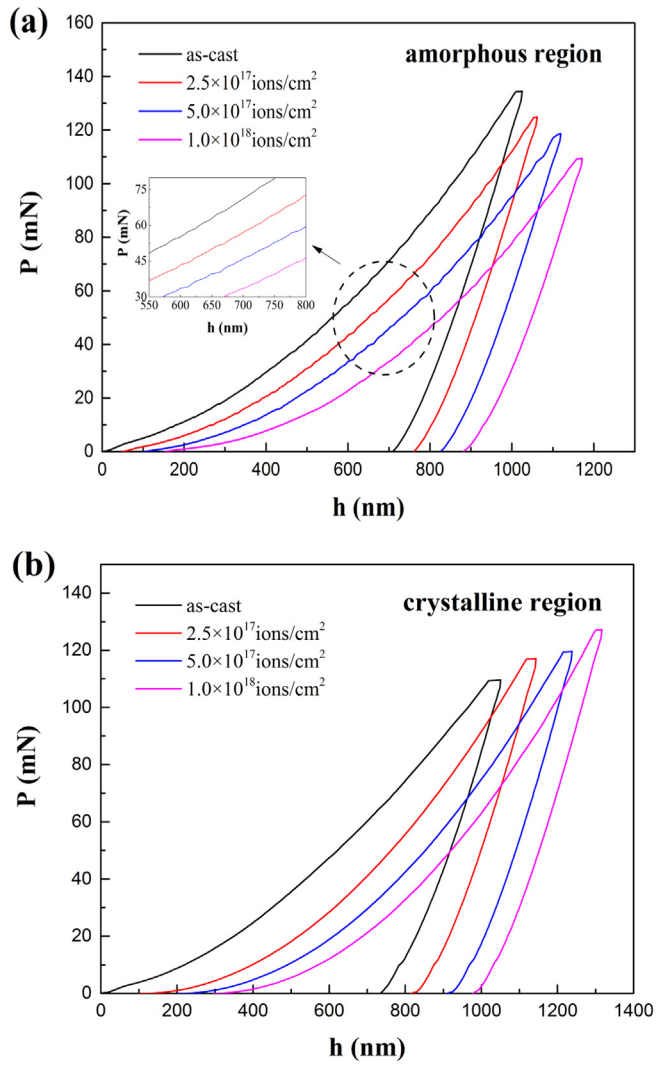

Fig. 6. Representative load-displacement (P-h) curves of nanoindentation texts of the amorphous and crystalline regions of $Cu_{48}Zr_{48}Al_4$ BMGC before and after irradiation. The insets show the enlarged view of the serration region.

increases, the formation of numerous nanocrystals leads to the decrease of the ductility. The results show that the amorphous atoms underwent a significant number of knock-on events, which can alter the structure by increasing the free volume, thereby improving the plasticity of the amorphous matrix, but the formation of helium bubbles and nanocrystals can reduce the ductility of BMGs [9,29].

4. Conclusion

In this study, the effect of He^+ ion irradiation on the structure and the mechanical properties of the $Cu_{48}Zr_{48}Al_4$ BMGC containing a B2-CuZr phase were investigated. The B2 phase was transformed into B19′ and B33 phases after irradiation. The irradiation induced the surface relief phenomenon, which was observed in the crystalline region. The RMS roughness of the sample surface increased significantly as the dose increased. The dose of 1×10^{18} ions/cm^2 resulted in cracking, exfoliation, and other irradiation damage that appeared on the surface. The irradiation damage in the crystalline region was more severe than in the amorphous region. The surface hardness and Young's modulus of the amorphous region showed various degrees of decline, as the irradiation increased the free volume inside the matrix and formed additional atomic scale defects. The surface hardness and Young's modulus were enhanced in the crystalline region, due to the formation of the martensitic phases. The macroscopic hardness of the $Cu_{48}Zr_{48}Al_4$ BMGC presented similar values after irradiation. These materials could maintain the stability of the mechanical properties under a certain critical irradiation dose, which could promote its application in the irradiation environment.

Acknowledgments

The authors would like to acknowledge the support by the National Natural Science Foundation of China (Grant No. 51401028, No. 51271193, No. 11402277, No. 11790292) and the Strategic Priority Research Program of the Chinese Academy of Sciences (Grant No. XDB22040303). The authors also thank to the support of Opening Fund of State Key Lab of Nuclear Physics and Technology at Peking University.

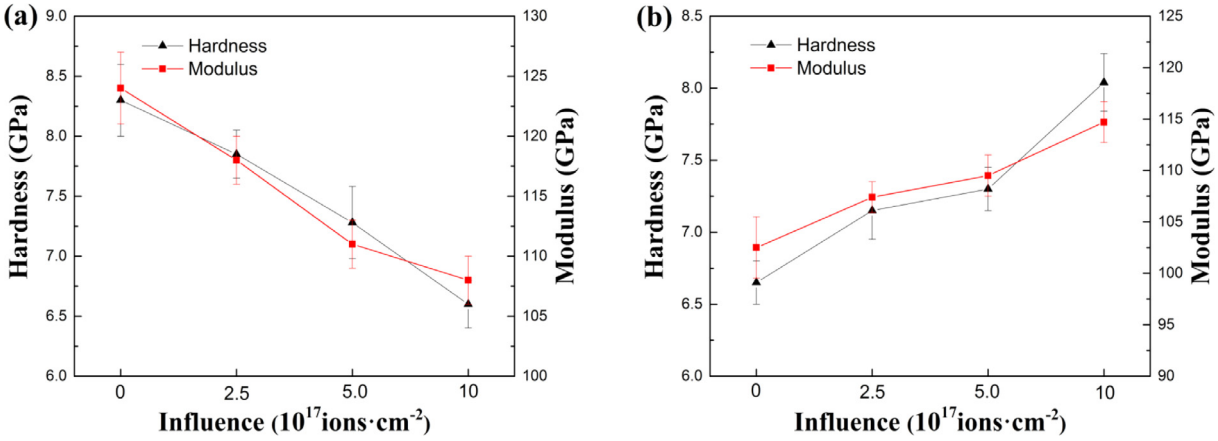

Fig. 7. Hardness (H) and Young's modulus (E) of (a) the amorphous region and (b) the crystalline region of as-cast and irradiated samples. (The experimental error bars in Fig. 7 are below 5%.)

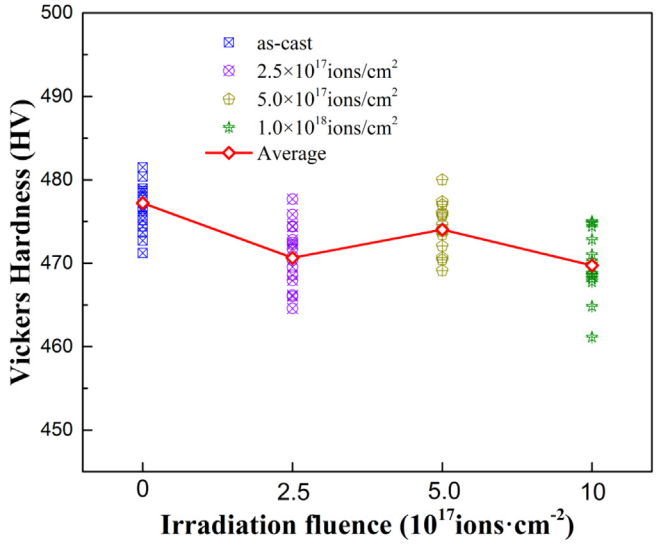

Fig. 8. The Vickers hardness (HV) of the $Cu_{48}Zr_{48}Al_4$ BMGC before and after irradiation at different doses.

References

[1] M. Okada, T. Noda, F. Abe, J. Nucl. Mater. 169 (1989) 249–256.
[2] S.B. Gilliam, S.M. Gidcumb, N.R. Parikh, D.G. Forsythe, B.K. Patnaik, J.D. Hunn, L.L. Snead, G.P. Lamaze, J. Nucl. Mater. 347 (2005) 289–297.
[3] S.A. Fabritsiev, A.S. Pokrovsky, S.J. Zinkle, A.F. Rowcliffe, D.J. Edwards, F.A. Gamer, V.A. Sandakov, B.N. Singh, V.R. Barabash, J. Nucl. Mater. 233–237 (1996) 526–533.
[4] T. Miyazawa, T. Nagasaka, R. Kasada, Y. Hishinuma, T. Muroga, H. Watanabe, T. Yamamoto, S. Nogami, M. Hatakeyama, J. Nucl. Mater. 455 (2014) 440–444.
[5] R.L. Klueh, K. Shiba, M.A. Sokolov, J. Nucl. Mater. 377 (2008) 427–437.
[6] J. Schroers, Adv. Mater. 22 (2010) 1566–1597.
[7] K. Zhang, Z. Hu, F. Li, et al., Appl. Surf. Sci. 390 (2016) 941–945.
[8] X. Mei, B. Wang, C. Dong, F. Gong, Y. Wang, Z. Wang, Nucl. Instrum. Methods Phys. Res., Sect. B 307 (2013) 11–15.
[9] X.L. Bian, G. Wang, H.C. Chen, et al., Acta Mater. 106 (2016) 66–77.
[10] C.A. Schuh, T.C. Hufnagel, U. Ramamurty, Acta Mater. 55 (2007) 4067–4109.
[11] D.C. Hofman, Science 329 (2010) 1294–1295.
[12] Y. Wu, Y.H. Xiao, G.L. Chen, C.T. Liu, Z.P. Lu, Adv. Mater. 22 (2010) 2770–2773.
[13] J.F. Ziegler, M.D. Ziegler, J.P. Biersack, Nucl. Instrum. Methods Phys. Res. B 268 (2010) 1818–1823.
[14] R. Limbach, B.P. Rodrigues, L. Wondraczek, J. Non-Cryst, Solids 404 (2014) 124–134.
[15] G.W. Egeland, J.A. Valdez, S.A. Maloy, K.J. McClellan, K.E. Sickafus, G.M. Bond, J. Nucl. Mater. 435 (2013) 77–87.
[16] A.Y. Konobeyev, U. Fischer, Y.A. Korovin, et al., Nucl. Eng. Technol. 3 (2017) 169–175.
[17] J. Carter, E.G. Fu, G. Bassiri, et al., Nucl. Instrum. Methods Phys. Res. B 267 (2009) 1518–1521.
[18] G. Xie, L. Shao, D.V. Louzguine-Luzgin, et al., Surf. Coat. Technol. 206 (2011) 829–833.
[19] C.A. Volkert, J. Appl. Phys. 74 (1993) 7107–7113.
[20] K. Zhang, Z. Hu, Z. Zhao, et al., Appl. Surf. Sci. 437 (2018) 176–180.
[21] J.P. Hirth, G. Spanos, M.G. Hall, H.I. Aaronson, Acta Mater. 46 (1998) 857–868.
[22] J.W. Seo, D. Schryvers, Acta Mater. 46 (1998) 1177–1183.
[23] W.H. Gao, X.Y. Yi, B. Sun, X.L. Meng, W. Cai, L.C. Zhao, Acta Mater. 132 (2017) 405–415.
[24] S.G. Roberts, A.S. Booth, P.B. Hirsch, Mater. Sci. Eng., A 176 (1994) 91–98.
[25] Y.I. Golovin, V.I. Ivolgin, V.A. Khonik, K. Kiagawa, A.I. Tyurin, Scr. Mater. 45 (2001) 947–952.
[26] R. Raghavan, B. Kombaiah, M. Dobeli, R. Erni, U. Ramamurty, J. Michler, Mat. Sci. Eng. A 532 (2012) 407–413.
[27] J.W. Seo, D. Schryvers, Acta Mater. 46 (1998) 1165.
[28] K.K. Song, S. Pauly, Y. Zhang, P. Gargarella, R. Li, N.S. Barekar, U. Kühn, M. Stoica, J. Eckert, Acta Mater. 59 (2011) 6620–6630.
[29] R. Liontas, X.W. Gu, E. Fu, et al., Nano Lett. 14 (2014) 5176–5183.
[30] D.Z. Chen, D. Jang, K.M. Guan, et al., Nano Lett. 13 (2013) 4462–4468.